Journal of Alloys and Compounds 509 (2011) 6337–6345

Contents lists available at ScienceDirect

Journal of Alloys and Compounds

journal homepage: www.elsevier.com/locate/jallcom

Structural and thermoelastic properties of $CaTiO_3$ perovskite between 7 K and 400 K

Kevin S. Knight [a,b,*]

[a] ISIS Facility, STFC Rutherford Appleton Laboratory, Harwell Oxford, Didcot, Oxon, OX11 0QX, UK
[b] Department of Mineralogy, The Natural History Museum, Cromwell Road, London, SW7 5BD, UK

ARTICLE INFO

Article history:
Received 4 February 2011
Received in revised form 28 February 2011
Accepted 2 March 2011
Available online 10 March 2011

Keywords:
$CaTiO_3$
Thermal expansion coefficient
Grüneisen parameter
Debye temperature
Symmetry-adapted basis-vector

ABSTRACT

The structural and thermoelastic properties of $CaTiO_3$ perovskite have been studied using high-resolution powder neutron diffractometry at eighty temperatures in the range 7–400 K. The temperature variation of the unit cell volume, the thermodynamic Grüneisen parameter and the isobaric heat capacity are analysed using a two-term Debye model. Structural parameters are presented as the magnitudes of symmetry-adapted basis-vectors of seven normal modes with wavevectors that lie on the surface of the Brillouin zone of the primitive cubic aristotype phase, and a structural basis for the temperature-dependence of the bond lengths is proposed. A consistency between the vibrational Debye temperatures derived from the atomic displacement parameters and the mean values of the vibrational energies of the three atomic species calculated from the partial phonon densities of states has been found.

1. Introduction

The structural phase transitions in the archetype perovskite $CaTiO_3$ [1–4], and the effect of substitution of Sr for Ca in the solid solution $Ca_{1-x}Sr_xTiO_3$ [5,6] remains a continuing challenge in structural physics. In the former case, this is due to the high temperatures required, and in the latter case, due to the unexpected, and as yet unexplained complex superlattice associated with the T point of the primitive cubic Brillouin zone for compositions around $x \sim 0.6$. The nature of the phase transitions remains controversial, in particular the region between 1486 K and 1523 K. Below 1486 K the space group is demonstrably orthorhombic *Pbnm*, and above 1523 K the space group is found to be tetragonal, *I*4/*mcm* [4]. The orthorhombic space group *Cmcm* had been proposed by Kennedy et al. [2] for this intermediate phase, but this has been discredited by the most recent work of Yashima and Ali [4]. However there still remain unexplained lattice parameter anomalies that have been observed at the highest crystallographic resolution by powder neutron diffraction in $CaTiO_3$ [7], the Ca-rich end of the $Ca_{1-x}Sr_xTiO_3$ solid solution [6], and the Ti-rich end of the perovskite – brownmillerite $CaTi_xFe^{III}{}_{1-x}O_{3-x/2}$ solid solution [8]. With the exceptions of the neutron diffraction and elasticity studies of the Sr-rich end of the $Ca_xSr_{1-x}TiO_3$ solid solution [6,9], there have been disappointingly few low-temperature studies of the physical properties of the $CaTiO_3$ end member. Of these, perhaps the most interesting are the low-temperature dielectric studies that have shown that $CaTiO_3$, like $SrTiO_3$, behaves as an incipient ferroelectric, with a TO polar soft mode [10].

In addition to acting as a model system in which to study zone-boundary structural phase transitions, $CaTiO_3$ perovskite has found practical application as a host phase for transuranic elements in the high-level waste disposal/immobilisation SYNROC ceramic. The understanding and measurement of phase equilibria, phase stability and thermoelastic properties of transuranic element containing $CaTiO_3$ is therefore of great importance in the nuclear industry [11–15]. In this paper we investigate the low temperature structural evolution of the parent phase $CaTiO_3$ and determine a set of thermoelastic properties in the framework of a modified Debye model.

2. Experimental and data analysis

~13 g of polycrystalline $CaTiO_3$ (Sigma Aldrich), annealed at 1500 K for 2 days, was loaded into a 15 mm thick aluminium sample can of slab geometry with thin, neutron-transparent, vanadium front and back windows. Heat could be supplied to the sample through a 100 W cartridge heater inserted into one wall of the sample container, and control thermometry was provided by a Rh-Fe sensor inserted into the opposite wall. Good thermal contact between the sample container and the heater and sensor was

* Correspondence address: ISIS Facility, STFC Rutherford Appleton Laboratory, Harwell Oxford, Didcot, Oxon, OX11 0QX, UK. Tel.: +44 1235 445220; fax: +44 1235 445720.
E-mail address: Kevin.knight@stfc.ac.uk

0925-8388/$ – see front matter © 2011 Elsevier B.V. All rights reserved.
doi:10.1016/j.jallcom.2011.03.014

Table 1
Structural parameters for $CaTiO_3$ perovskite at 7 K.

		$CaTiO_3$
Lattice parameters (Å)	a	5.36773(3)
	b	5.43367(3)
	c	7.62686(4)
Unit cell volume (Å^3)		222.448(1)
Ca	x	0.0063(2)
	y	0.5378(1)
	$100u_{iso}$ (Å^2)	0.48(2)
Ti	$100u_{iso}$ (Å^2)	0.35(20
O1	x	−0.0738(1)
	y	−0.0171(1)
	$100u_{eq}$ (Å^2)	0.46(4)
O2	x	0.2096(1)
	y	0.2896(1)
	z	0.0381(1)
	$100u_{eq}$ (Å^2)	0.51(3)
Rp[a]		0.051
Rwp[a]		0.044

Space group: *Pbnm*. Ca, O1: 4*c* *x*, *y*, 1/4. Ti: 4*a* 0, 0, 0. u_{eq} is defined as 1/3 the trace of the diagonalised atomic displacement parameter matrix.

[a] 4609 observations and 41 variables.

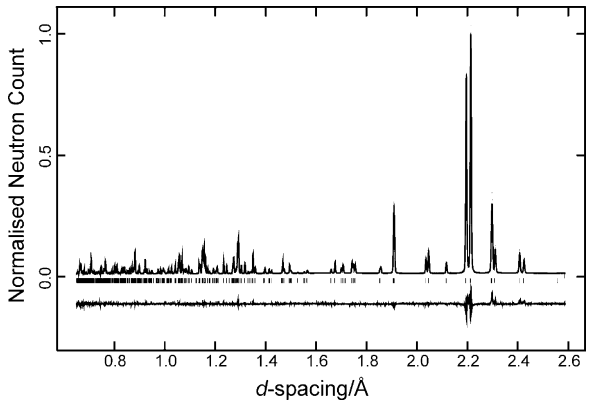

Fig. 1. Rietveld fit to the 7 K data of $CaTiO_3$ perovskite. Observed data are shown as ●, calculated as the full black line, reflection markers as vertical ticks. The difference (observed – calculated) is shown as the full black line below the reflection markers.

achieved using a copper-based anti seize compound. The sample was directly heated to 400 K in a Sumitomo RDK-415D top loading CCR under 30 mbar of helium exchange gas. Powder neutron diffraction data were collected in time-of-flight from 30 ms to 130 ms using the high resolution backscattering detector bank of the HRPD diffractometer at the ISIS neutron spallation source. Data were collected at 400 K, 395 K, and in 5 K steps to 10 K, with

Table 2
Lattice parameter fitting coefficients, 7 K ≤ T ≤ 400 K.

	$CaTiO_3$
(a)	
l_0 (Å)	5.36790(3)
k (Å)	0.0274(3)
Θ (K)	325(3)
(b)	
l_0 (Å)	5.43372(1)
k_1 (Å)	0.0027(3)
Θ_1 (K)	191(12)
k_2 (Å)	0.027(2)
Θ_2 (K)	934(40)
(c)	
l_0 (Å)	7.62685(2)
k_1 (Å)	0.0166(1)
Θ_1 (K)	234(7)
k_2 (Å)	0.0322(1)
Θ_2 (K)	776(49)

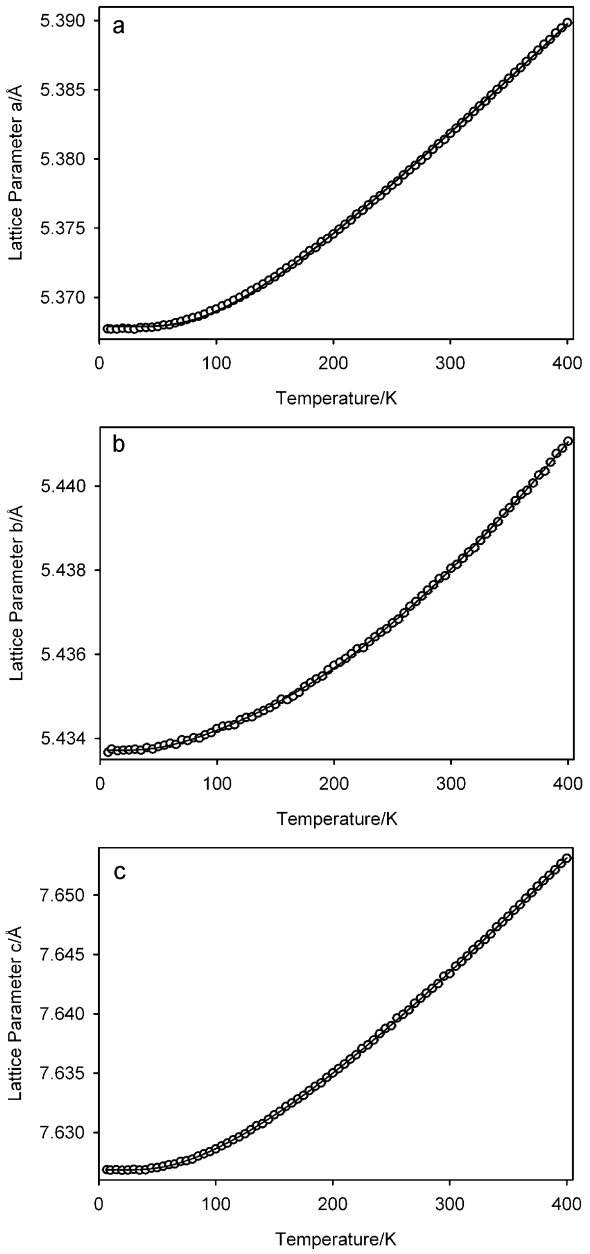

Fig. 2. The temperature-dependence of the lattice parameters of $CaTiO_3$ for 7 K ≤ T ≤ 400 K. For the lattice parameter a, (a), the full line shows the fit to a single term expression, for the lattice parameters b and c, (b) and (c), the full line shows the fit to a two-term expression; both are defined in the text. The estimated standard deviations for all points in all graphs are less than the size of the plotting symbol.

a final measurement being made at 7 K. With the exceptions of the 400 K and 7 K runs, which were measured for 80 μAh incident proton beam current, all other measurements were made for 10 μAh, approximately 13 min duration. Once the control sensor had reached the set point temperature, data collection was commenced after a 3 min thermal equilibration period; thermal stability was of the order ±0.2 K for all data collection temperatures.

The neutron time-of-flight data were focused, normalised to the incident flux distribution and corrected for self shielding and wavelength-dependent absorption for a sample with measured number density of 9.3×10^{21} cm^{-3} and calculated cross sections of 19.88 b for scattering, and 6.52 b at 1.798 Å, for wavelength-dependent absorption. Data in the time-of-flight range 32–120 ms, corresponding to a d-spacing range of ~0.64–2.4 Å, were analysed using the GSAS package [16]. The initial starting model for the crys-

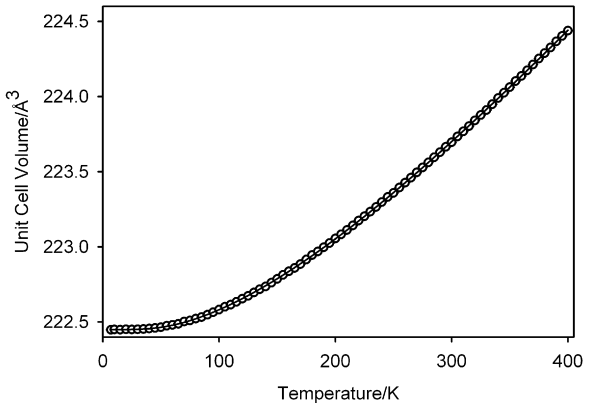

Fig. 3. The temperature-dependence of the unit cell volume of $CaTiO_3$ for $7\,K \leq T \leq 400\,K$. The full line shows the fit to the data according to a two-term Debye internal energy function described in the text.

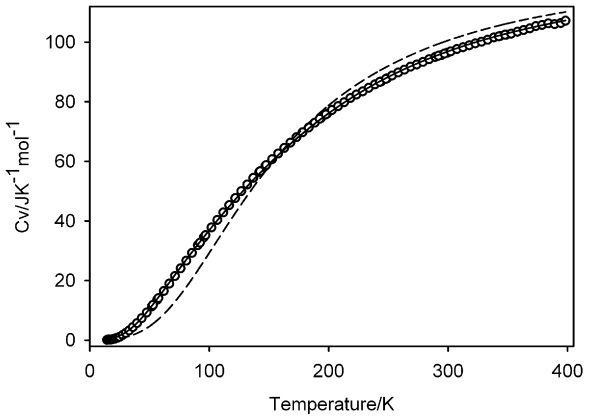

Fig. 4. The isochoric heat capacity of $CaTiO_3$ for $7\,K \leq T \leq 400\,K$ calculated from the isobaric heat capacity of Woodfield et al. [24] using the temperature-dependent molar volume and thermal expansion coefficient from the fitting of the unit cell data, and the bulk modulus of Ross and Angel [23]. The dashed line shows the fit to these data according to a Debye model, the full line shows the fit to the modified two-term Debye model of Barron [22].

tal structure refinement from the 400 K data was the 298 K solution of Knight [17]. Convergence from this solution was rapid for a model with isotropic atomic displacement parameters for the cations, and anisotropic atomic displacement parameters for the anions. The result from the 400 K refinement was used as the initial model for

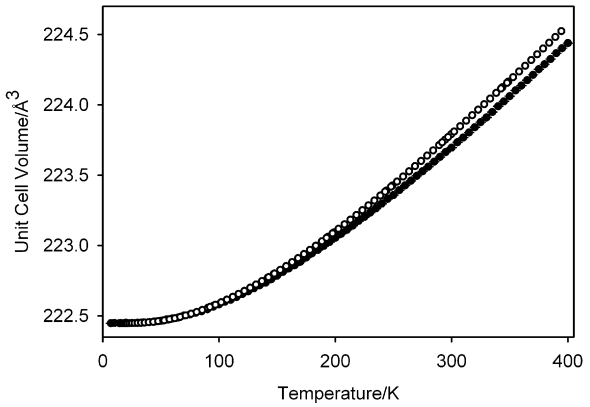

Fig. 5. The calculated temperature dependence of the unit cell volume (●) based on the two-term Debye internal energy functions derived from the isobaric heat capacity of Woodfield et al. [24], assuming a temperature independent bulk modulus. The observed temperature dependence of the unit cell volume (○) calculated from the fitting coefficients of the unit cell using the two-term Debye model.

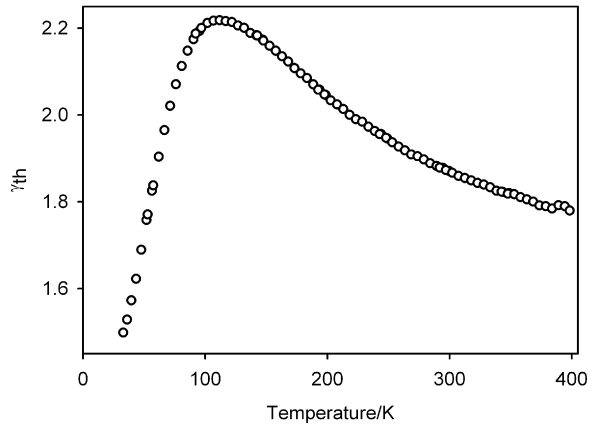

Fig. 6. The temperature dependence of the thermodynamic Grüneisen parameter for $CaTiO_3$ perovskite.

the 395 K refinement, and the whole procedure was carried out iteratively down to the 7 K refinement. Typical results, in this case from the 7 K refinement, are listed in Table 1, and the quality of fit is shown in Fig. 1.

3. Results and discussion

3.1. Thermoelastic properties

The temperature variation of the lattice parameters for $CaTiO_3$ are shown in Fig. 2 and exhibit the expected Grüneisen behaviour for a dielectric; saturation at the lowest temperature, and a constant thermal expansion coefficient at the highest temperatures measured. The data show no evidence for the condensation of the soft polar TO mode which might be visible as lattice parameter anomalies. The extent of the saturation region is approximately constant for the *a* and *c* axes (*a*, 58 K; *b*, 88 K; *c*, 56 K), although the three individual high temperature axial thermal expansion coefficients are quite different. Each lattice parameter was fitted to an empirical expression of the form $l(T) = l_0 + k/(\exp(\theta/T) - 1)$, shown as the full line in the case of $a(T)$, however this expression proved inadequate for the *b* and *c* axes, failing to fit in the temperature region where the lattice parameter moves off the saturation base-line. The full lines on the figure for $b(T)$, and $c(T)$, are the results of fitting to an empirical two-term expression $l(T) = l_0 + k_1/(\exp(\theta_1/T) - 1) + k_2/(\exp(\theta_2/T) - 1)$, which is excellent over the whole of the measured temperature range. In the absence of ferroelastic structural phase transitions which modify the thermal expansion behaviour, the high temperature axial thermal expansion coefficients can be estimated from the fitted parameters, which are listed in Table 2, where $(1/l_0)\mathrm{d}l/\mathrm{d}T = 1/l_0 \sum_i k_i/\theta_i$. For temperatures below the *Pbnm* – *I*4/*mcm* phase transition temperature, the predicted high temperature axial thermal expansion coefficients, $\alpha_a = 1.57 \times 10^{-5}\,K^{-1}$, $\alpha_b = 7.9 \times 10^{-6}\,K^{-1}$, $\alpha_c = 1.47 \times 10^{-5}\,K^{-1}$, are in good agreement with the experimental measurements of Ball et al. [18], Sato et al. [12] and Redfern [19]. However, as this phase transition temperature is approached, all three axial thermal expansion coefficients are found by experiment to increase significantly [7], and the agreement with prediction is poor.

Transforming the orthorhombic lattice parameters via the matrix (1/2 −1/2 0/1/2 1/2 0/0 0 1/2) to the pseudocubic subcell ($a_p = b_p \neq c_p$; $\alpha_p = \beta_p = 90°$, $\gamma_p \neq 90°$), an estimation of the *Pbnm* – *I*4/*mcm* phase transition temperature can be made from the temperature dependence of the shear angle γ_p which extrapolates to 90° at a temperature of 1342 K, close to the temperature interval 1373–1423 K for this transition reported by Redfern [19]. How-

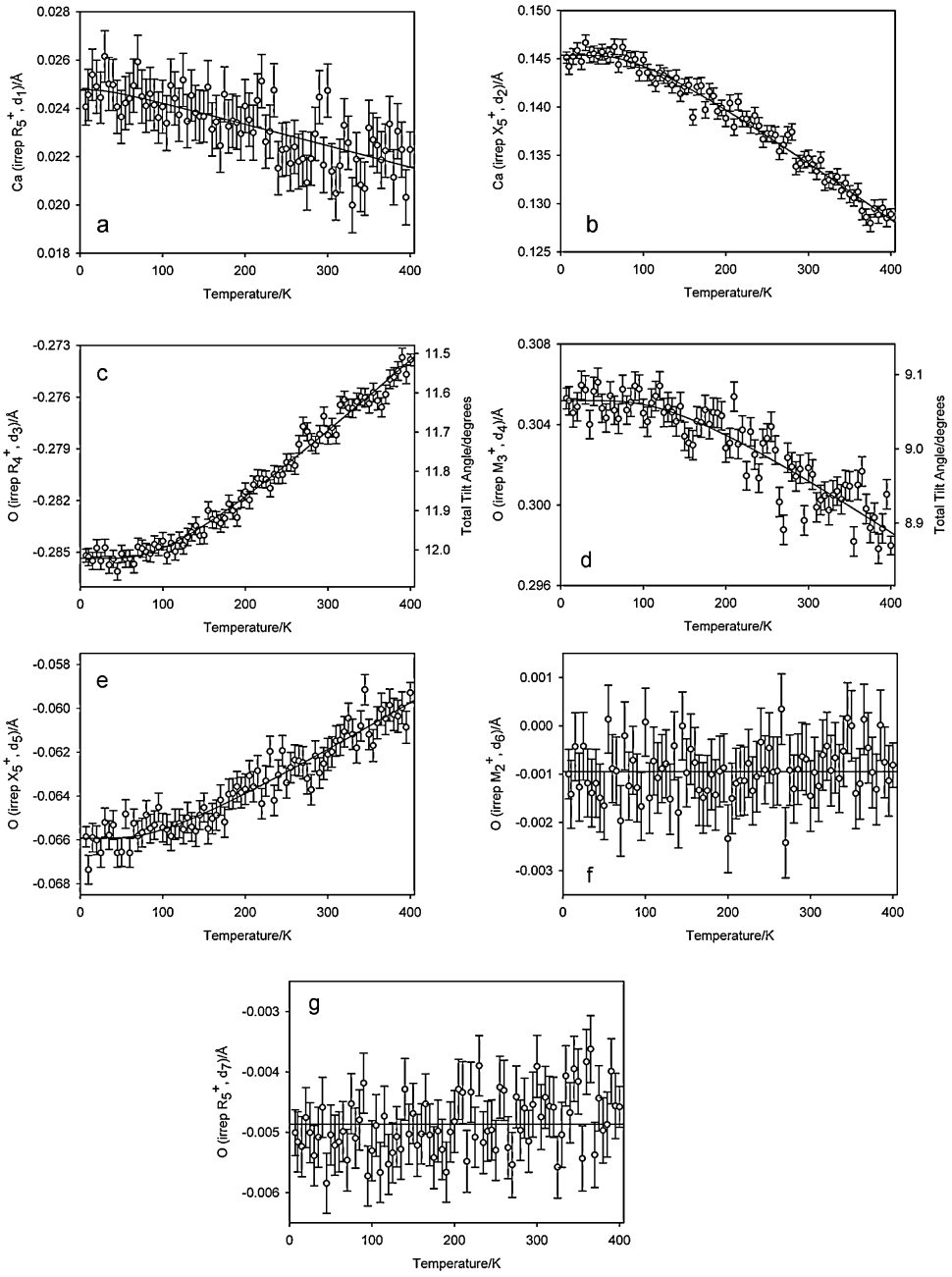

Fig. 7. The temperature dependence of the seven symmetry-adapted basis-vectors consistent with space group *Pbnm*. The cation displacemens are shown in (a) and (b), the anion displacements in (c)–(g). The octahedral tilting modes, (c) and (d), that form the primary oder parameters in this space group are shown with their corresponding full tilt angles on the right-hand ordinate axis. The octahedral distortion modes are shown in (e)–(g), where the mode that transforms as the irreducible representation M_2^+ has close to zero magnitude over the entire temperature range. Basis-vector labelling follows Knight [17].

ever, as noted earlier, there remains significant disagreement in the literature as to the precise transition temperatures for the two high-temperature structural phase transitions in $CaTiO_3$ [4,6]. Values for the spontaneous strains e_4, e_{tx} and e_a, calculated using the cube root of one quarter of the temperature-dependent unit cell volume for the unstrained lattice parameter $a_0(T)$, were in close agreement with those evaluated for $CaTiO_3$ at 400 K by Carpenter et al. [20].

The temperature dependence of the unit cell volume is shown in Fig. 3 and has a similar behaviour to the unit cell axes, saturation from the lowest temperature to ~50 K, a slow increase with increasing temperature, before exhibiting a nearly constant thermal expansion coefficient at temperatures greater than ~300 K. Assuming a Grüneisen approximation to the zero-pressure equation of state, for low temperatures the molar volume varies as the internal energy $U(T)$ [21], $V(T) = V_0 + (\gamma/K_0)U(T)$, where γ is a Grüneisen parameter and K_0 is the isothermal bulk modulus. For a Debye internal energy function, the molar volume is given by:

$$V(T) = V_0 + \frac{9\gamma N K_B T}{K_0}\left(\frac{T}{\Theta_D}\right)^3 \int_0^{\Theta_D/T} \frac{x^3}{e^x - 1} dx$$

where θ_D is the Debye temperature, N is the number of atoms in volume V_0, and K_B is Boltzmann's constant. A fit to the unit cell volume according to this expression fits the lowest- and highest-temperature regions well ($V_0 = 222.461(2)$ Å^3, $\Theta_D = 473(5)$ K, $(\gamma/K_0) = 9.51 \times 10^{-12}$ Pa^{-1}, $r^2 = 0.99905$), but is inadequate for the intermediate temperature range. Extending the

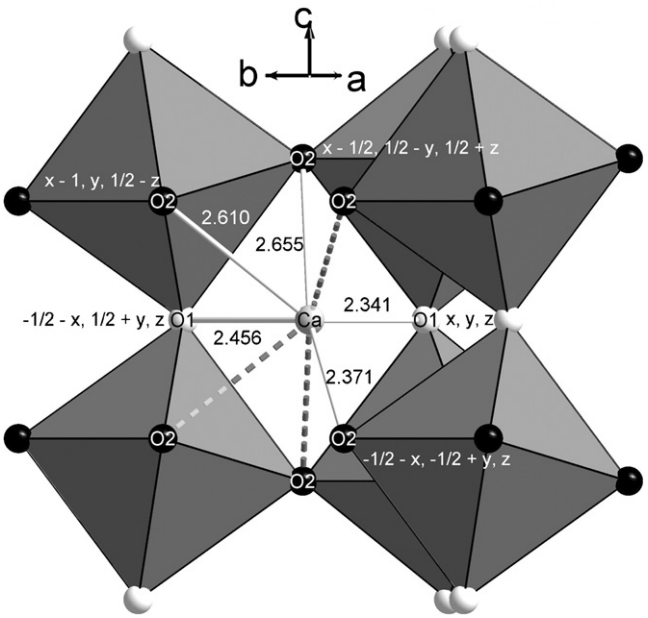

Fig. 8. The bonding environment of the CaO_8 polyhedron centred on the Ca with fractional coordinate $(-1/2-x, -1/2+y, 1/2-z)$. The five symmetry independent bonds are shown with full lines and the fractional coordinates of the coordinating anions. Ca – O1 $(-1/2-x, 1/2+y, z)$ is labelled as bond b_3; Ca – O1 (x, y, z) b_2; Ca – O2 $(x-1, y, 1/2-z)$ b_9; Ca – O2 $(-1/2-x, -1/2+y, z)$ b_5; Ca – O2 $(x-1/2, 1/2+y, 1/2+z)$ b_{11}. Bond labelling follows Knight [30].

Debye model to allow for two separate speeds of sound [22], the molar volume is given by $V(T) = V_0 + (\gamma_1/3K_0)U_1(T) + (2\gamma_2/3K_0)U_2(T)$ with two effective Grüneisen parameters and Debye temperatures. The fit to this model is shown as the full line on Fig. 3 which can be seen to fit the whole temperature range well ($V_0 = 222.4475(6)$ Å^3, $\Theta_{D1} = 323(7)$ K, $(\gamma_1/K_0) = 1.79 \times 10^{-11}$ Pa^{-1}, $\Theta_{D2} = 1022(40)$ K, $(\gamma_2/K_0) = 7.1 \times 10^{-12}$ Pa^{-1}, $r^2 = 0.99999$). The weighted average of the two Debye temperatures, 789 K, is in excellent agreement with that determined from the longitudinal and shear sound velocities, 760(3) K [15]. Using a value of 170.9 GPa for the isothermal bulk modulus of $CaTiO_3$ [23], the Grüneisen parameters are found to be 3.1 and 1.2 for γ_1 and γ_2 respectively. At high temperatures, the volume thermal expansion coefficient is estimated to be 4.0×10^{-5} K^{-1}, close to three times the average linear thermal expansion coefficient measured by dilatometry in the temperature interval 298–1273 K [15].

The isochoric molar heat capacity of $CaTiO_3$, C_V, was calculated from the experimentally determined isobaric heat capacity, C_P [24], using results for the temperature-dependence of the molar volume and thermal expansion coefficient from the modified Debye model described above. Fig. 4 shows the isochoric heat capacity and two fits according to Debye internal energy functions. The dashed line shows the fit to the data for a Debye internal energy function,

$$C_V(T) = 9NK_B T\left(\frac{T}{\Theta_D}\right)^3 \int_0^{\Theta_D/T} \frac{x^4 e^x}{(e^x-1)^2}\,dx$$

from which the Debye temperature was determined as 637(7) K which is in fair agreement with the Debye temperature of 583 K calculated from the lowest five values of the isobaric heat capacity [24] and assuming a T^3 temperature dependence. However, It is clear from the figure, that at low temperatures there are more active modes than the simple Debye model predicts, whilst at high temperatures, the opposite is found to be true. The full line on the figure shows the results of fitting the isochoric heat capacity to the modified Debye model of Barron [22] that allows for two independent cut off frequencies and Debye temperatures, whilst retaining the high temperature Dulong–Petit limit.

$$C_V(T) = \frac{1}{3}C_{V1}(T) + \frac{2}{3}C_{V2}(T).$$

The lower Debye temperature determined from fitting the isochoric heat capacity to this model, 317(4) K, is in good agreement with the lower Debye temperature determined from fitting the molar volume 323(7) K. The higher Debye temperature derived from fitting the heat capacity, 841(4) K, is however significantly less than that determined from fitting the molar volume, 1022(40) K.

By integrating the individual isochoric Debye heat capacity contributions, the molar volume was calculated using $V(T) = V_0 + (\gamma_1/3K_0)U_1(T) + (2\gamma_2/3K_0)U_2(T)$ and is shown in Fig. 5, where it can be seen that at low temperatures the difference between the observed and calculated volumes is small, but as the temperature increases, the difference becomes larger, but never more than 0.5%. All attempts to improve the agreement between the calculated and observed molar volumes, by fitting the data using the temperature-dependent bulk modulus model of Varshni [25], were unsuccessful, with the ambient-temperature bulk modulus being found to be 10% larger than the experimental determination [9,23]. It is probable that the discrepancy in the calculated and observed molar volumes arises from the assumption of a temperature-independent bulk modulus on the conversion of the isobaric heat capacity to the isochoric heat capacity.

The temperature variation of the thermodynamic Grüneisen parameter, γ_{th}, is shown in Fig. 6 calculated using the molar volume, V_m, and volume expansivity, α, from the modified Debye model used to fit the unit cell volume.

$$\gamma_{th}(T) = \frac{\alpha(T)K_0 V_m(T)}{C_V(T)}$$

γ_{th} rises steeply with increasing temperature to a maximum of ~2.2 at ~130 K, before decreasing at a much lower rate to ~1.8 by 400 K, with an average value of just under 2 for the whole temperature range. At room temperature, the value of γ_{th} is close to the weighted average of the two Grüneisen parameters derived from fitting the temperature-dependence of the unit cell volume (1.83), and is significantly higher than most other $A^{II}B^{IV}O_3$ perovskite-structured phases: $BaHfO_3$ (0.83), $BaSnO_3$ (1.37), $BaZrO_3$ (0.97), $BaUO_3$ (0.99), $BaCeO_3$ (1.92), $BaMoO_3$ (1.39), $SrHfO_3$ (1.27), $SrRuO_3$ (1.56), $SrMoO_3$ (1.06), $SrCeO_3$ (0.81); all calculated from thermoelastic data given in Yamanaka et al. [13]. For terrestrial geophysical modelling, Anderson has argued that the thermoelastic properties of the dominant lower mantle phase $MgSiO_3$ perovskite in space group *Pbnm* can be treated as a simple Debye solid, reporting a Grüneisen parameter for this phase of 1.52 [26].

3.2. Structural behaviour

Using the measured lattice parameters, the fractional coordinates at each temperature were decomposed into the magnitudes of the seven, orthogonal, symmetry-adapted basis-vectors of the aristotype phase that are consistent with the space group setting *Pbnm* [17]. The displacement of the Ca cation in the direction of the orthorhombic *a* axis is the vector sum of two basis-vectors of equal magnitude that transform as the irreducible representation (irrep) R_5^+ of the cubic aristotype phase, whilst the displacement in the orthorhombic *b* axis direction is associated with the vector sum of two basis-vectors of equal magnitude that transform as the irrep X_5^+. The temperature-dependences of these two modes is illustrated in Fig. 7a and b and shows that the displacement associated with the irrep X_5^+ is larger, by a factor of ~5.8 at 7 K, and has a more rapid reduction with increasing temperature than the displacement associated with the irrep R_5^+. To enable a structural basis to be derived for the temperature variations of the

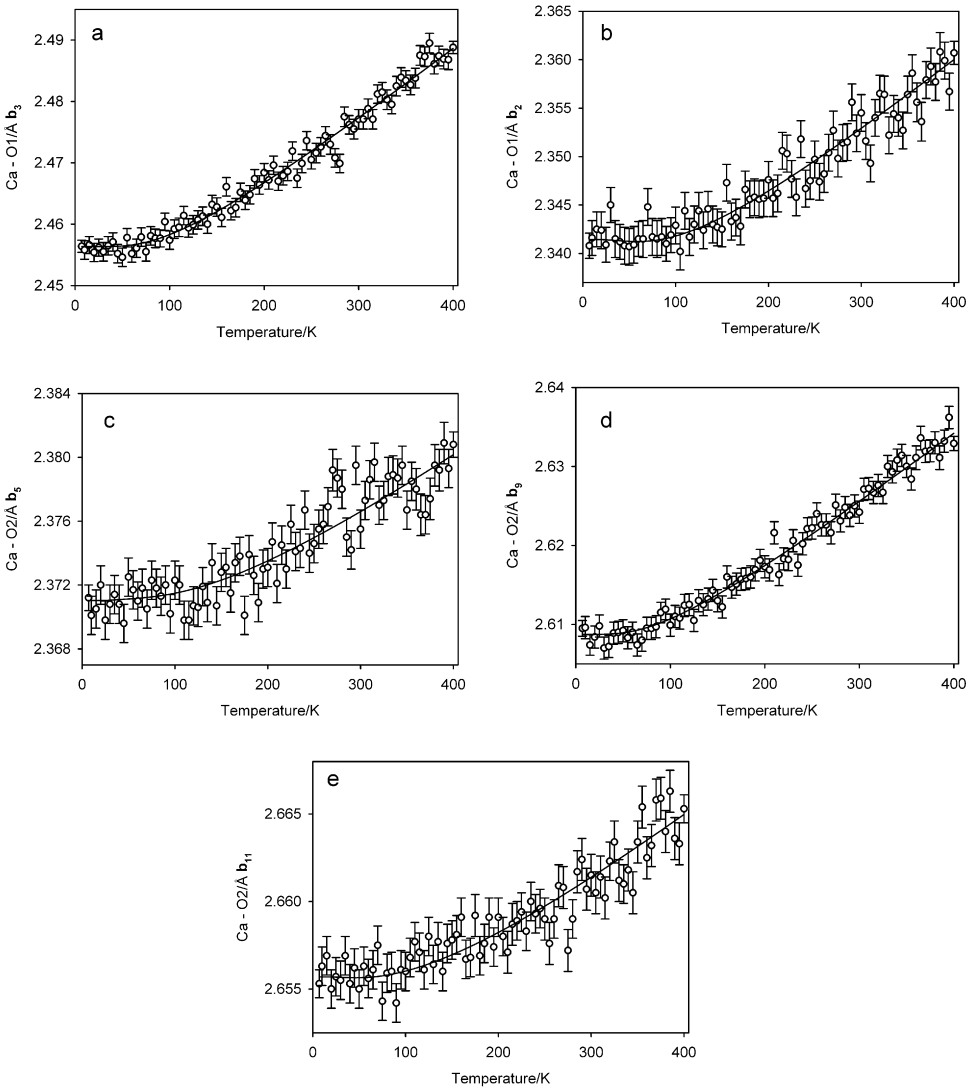

Fig. 9. The temperature dependence of the five symmetry independent bonds in the CaO_8 polyhedron. The full lines show the predicted behaviour of the bonds based on simple parameterisation of the temperature variation of the symmetry-adapted basis-vector amplitudes.

bond lengths, these two modes, and the three associated with the deformation and rotation of the octahedron, have been empirically parameterised using the same expression as used for fitting the *a* lattice parameter, and these are shown on these figures as full lines. Both modes extrapolate to zero magnitude i.e. the ideal fractional coordinate for the A-site cation at physically unreasonable temperatures, well above the 1 atm. melting temperature of 2262 K [12].

The primary order parameters for a perovskite-structured compound in space group *Pbnm* are associated with the in-phase and anti-phase tilting modes that transform as the irreps M_3^+ and R_4^+ respectively [27]. In addition to these two modes, the octahedron is potentially deformed from ideality by modes that transform as the irreps X_5^+, M_2^+ and R_5^+ [17,28,29]. At all measured temperatures, the magnitudes of the tilting modes are larger than the octahedral deformation mode with irrep X_5^+, whilst the amplitudes associated with deformation the modes with irreps M_2^+ and R_5^+ are very small and constant. On the basis of a limited survey of ambient temperature perovskite crystal structures in space group *Pbnm*, Knight has argued that unless the B-site cation permits a Jahn–Teller distortion, the octahedral deformation from the mode that transforms as the irrep M_2^+ probably does not exist as a condensed mode [30]. Fig. 7c and d illustrate the temperature-dependence of the amplitudes of the two tilting modes and their related total tilt angles, whilst Fig. 7e–g show the amplitudes of the octahedral deformation modes, where in particular, the amplitude associated with the irrep M_2^+ is zero within 1 and 2 estimated standard deviations at all temperatures. For subsequent discussions of the temperature-dependence of the bond lengths, the amplitudes of the basis-vectors are labelled as d_i ($i = 1, 7$) in Fig. 7.

The eightfold coordination of the Ca site $(-1/2 - x, y - 1/2, z)$ at 7 K is illustrated in Fig. 8 along with the lengths of the five symmetry independent bonds and the fractional coordinates of the bonded anions. Both the coordinated anions O1, and the Ca cation, lie on the mirror plane of the space group; the six anions O2 are in general positions, related in pairs through mirror symmetry. Bond labelling follows Knight [30]: Ca – O1 (x, y, z) b_2; Ca – O1 $(-1/2 - x, 1/2 + y, z)$ b_3; Ca – O2 $(-1/2 - x, -1/2 + y, z)$ b_5; Ca – O2 $(x - 1, y, 1/2 - z)$ b_9; Ca – O2 $(x - 1/2, 1/2 - y, 1/2 + z)$ b_{11}. After an initial saturation interval of <100 K, all five bonds, increase with increasing temperature, as shown in Fig. 9, however the high temperature bond thermal expansion coefficients are found to vary by a factor of ~3. The full lines on each figure are the predicted bond length variations based on the parameterisations of the amplitudes of the symmetry-adapted basis-vectors described earlier, and permit the determination of the structural basis for the bond expansion.

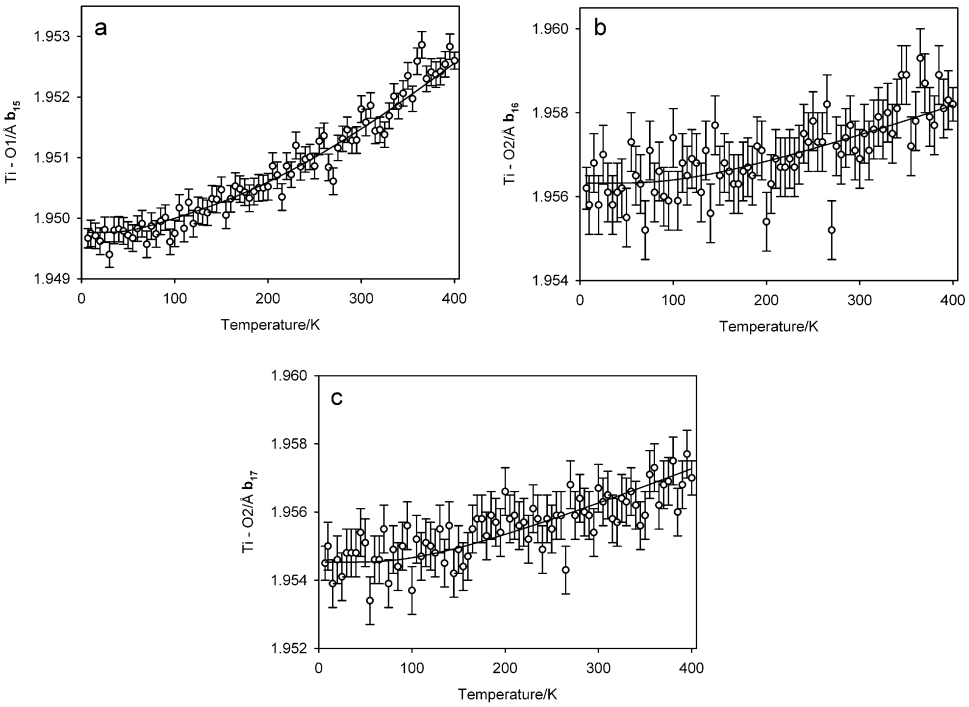

Fig. 10. The temperature dependence of the three symmetry independent bonds in the TiO_6 octahedron. The full lines show the predicted behaviour of the bonds based on simple parameterisation of the temperature variation of the symmetry-adapted basis-vector amplitudes. Bond labelling follows Knight [30].

For temperatures greater than ~400 K, the highest bond thermal expansion coefficient, $\sim 4.9 \times 10^{-5}\,K^{-1}$, is found for the bond b_3 lying in the mirror plane and arises principally from the Ca displacement mode d_2, with smaller contributions from the octahedral deformation mode d_5 and the thermal expansion of the *b* axis. Intermediate thermal expansion is found for two bonds, b_2 in the mirror plane, and b_9 out of the mirror plane, both having essentially identical bond thermal expansion coefficients of $\sim 3.4 \times 10^{-5}\,K^{-1}$. In the former case, the bond expansion of b_2 is principally related to the anti-phase octahedral tilt mode, d_3, and the thermal expansion of the *a* axis. The displacement of the Ca cation, modes d_1 and d_2, providing a significant bond-shortening contribution. In the latter case, the bond thermal expansion of b_9 is more complex, with the largest contribution arising from the Ca displacement mode d_2, but also the anti-phase tilting mode d_3, and to a lesser extent the thermal expansion of the *a* and *c* axes. The contribution from the in-phase tilt mode, d_4, is negative and of a magnitude similar to that from the anti-phase tilts. The bonds b_5 and b_{11} show the smallest high temperature thermal expansion coefficient of $\sim 1.5 \times 10^{-5}\,K^{-1}$. For bond b_5 there are large positive contributions arising from both the tilting modes d_3 and d_4, and to a lesser extent the thermal expansion of the *a* and *c* axes, but by far the largest individual contribution is negative and arises from the antipathetic displacement of the Ca cation, mode d_2. In the case of bond b_{11}, there are large positive contributions from the cation displacement mode d_2 and the three lattice parameters, but the overall expansion is halved by a reduction arising from the antiphase tilt displacement, d_3.

The thermal expansion coefficients of the Ti–O bonds, by comparison, are almost a factor of ten times smaller than the Ca–O bonds, and hence, are less easy to parameterise with confidence. The bonds are labelled using the nomenclature of Knight [30]. In the case of the Ti–O1 bond, b_{15}, the measured positive bond thermal expansion coefficient arises entirely from the thermal expansion of the *c* axis, but this overall effect is halved due to the negative contribution from the antiphase tilt mode, d_3. The thermal expansion coefficients of the two Ti–O bonds to anion O2 are both dominated by positive contributions from the *a* and *b* axes, but in the case of bond b_{16}, this is reduced by a very large negative component from the antiphase tilt mode d_3, which itself is partially offset by an additional positive component of the same mode. For bond b_{17}, an identical effect with an identical cause to that observed for b_{16} is seen, but in this case there is an additional negative contribution from the in-phase tilt mode d_4. The temperature dependence of the Ti–O bonds and their predicted behaviour based on the symmetry-adapted basis-vector parameterisation is shown in Fig. 10.

Below ~40 K, the TiO_6 and CaO_8 polyhedra exhibit constant volumes, but by temperatures of 100 K, there is a rapid increase in both polyhedral volumes with estimated high temperature limits of $1.5 \times 10^{-5}\,K^{-1}$ for the octahedral volume, and $5.1 \times 10^{-5}\,K^{-1}$ for the CaO_8 polyhedron. At all temperatures above saturation, the volume strain associated with the eightfold site exceeds that of the sixfold site reflecting the greater degrees of structural freedom available to, and the relative softness of the A site in the

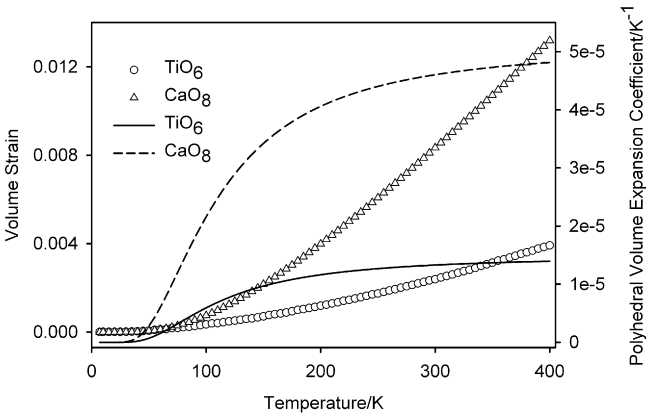

Fig. 11. The temperature variation of the polyhedral volume strains and their associated thermal expansion coefficients. The CaO_8 polyhedron shows a larger stain and greater thermal expansion coefficient that the TiO_6 octahedron at all temperatures above the saturation temperature reflecting the more open, less constrained cavity site.

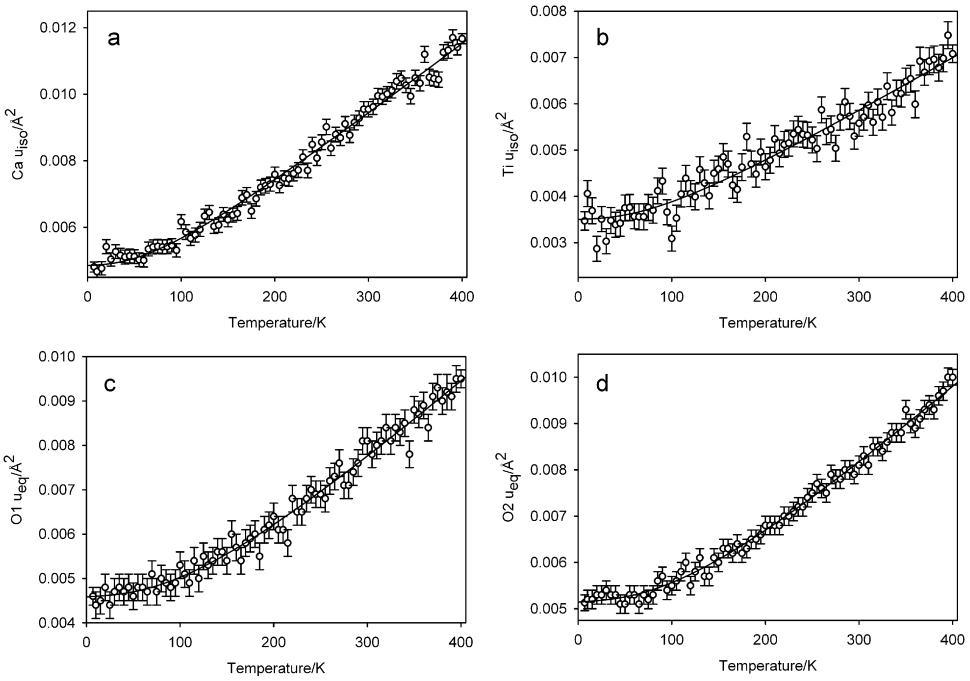

Fig. 12. The temperature dependence of the isotropic atomic displacement parameters for the cations ((a) and (b)) and the isotropic equivalent atomic displacement parameters of the anions ((c) and (d)). The full lines are fits to these data using the modified Debye model of Wood et al. [31].

perovskite structure. The volume strain and the calculated polyhedral thermal expansion coefficients for both polyhedra are shown in Fig. 11. Unsurprisingly, the bond angles within the TiO_6 octahedron exhibit little variation with increasing temperature, and only the O2–Ti–O2 angle shows a significant systematic reduction of ~0.06° in 400 K. The increase in volume of the octahedron is therefore primarily governed by the increase in the Ti–O bond lengths with temperature. By contrast, the temperature dependence of the bond angles within the CaO_8 polyhedron is complex, with bond angles increasing, decreasing or remaining invariant with increasing temperature. Increases/decreases in bond angles are found to be a factor of ~10 greater in the CaO_8 polyhedron than the equivalent changes observed in the TiO_6 octahedron. Knight has shown that it is possible to parameterise these bond angles in terms of the amplitudes of the symmetry-adapted basis-vectors [30], but the interpretation of cause and effect is difficult to disentangle with confidence due to the complexity of the expressions derived from the combination of scalar products.

The temperature variation of the atomic displacement parameters for the cations, or the equivalent isotropic atomic displacement parameters in the case of the anions, is shown in Fig. 12. The full line on each figure shows a fit to the data using the modified Debye model proposed by Wood in which the zero-point displacement parameter is permitted to be a refinable variable in addition to the vibrational Debye temperature [31].

$$\overline{u^2}(T) = \frac{3h^2T}{4\pi^2 M k_B \Theta_D^2}\varphi\left(\frac{\Theta_D}{T}\right) + A$$

$$\varphi\left(\frac{\Theta_D}{T}\right) = \left(\frac{T}{\Theta_D}\right)\int_0^{\Theta_D/T}\frac{x dx}{e^x - 1}$$

The zero point contribution for the Ca cation, $4.85(4)\times10^{-3}$ Å^2, is comparable to those of the anions, O1 $4.58(4)\times10^{-3}$ Å^2 and O2 $5.14(2)\times10^{-3}$ Å^2, and is significantly larger than that for the Ti cation, $3.50(6)\times10^{-3}$ Å^2, once again reflecting the more open eightfold coordination. In addition, there is a marked disparity between the refined vibrational Debye temperatures of the cations, Ca 410(2) K and Ti 503(6) K, when compared to the two anions, which are essentially identical, O1 695(4) K and O2 707(3) K.

The temperature-dependence of the molar volume and the isochoric heat capacity have been found to be consistent with a two-term Debye model in which the lower characteristic temperatures are in good agreement (V_m: Θ_{D1} = 323(7) K, C_V: Θ_{D1} = 317(4) K), although the higher characteristic temperatures agree less well (V_m: Θ_{D2} = 1022(40) K, C_V: Θ_{D2} = 841(4) K). This two term behaviour is mirrored in the vibrational Debye temperatures derived from fitting the atomic displacement parameters and is suggestive of the cations contributing more to the lower temperature Debye distribution, and the anions to the higher temperature distribution. The two-term Debye model proposed by Barron [22] separates the longitudinal contribution from the transverse contributions in the ratio of 1:2, which coincidentally, is close to the cation:anion ratio in perovskites of 2:3, and indeed, the icochoric heat capacity can be fitted almost as well by using mixing parameters of 2/5 and 3/5 rather than 1/3 and 2/3.

Ab-initio calculations [32] and molecular dynamics simulations [33] of the total and partial phonon density of states provide some evidence to support this simple model. The calculated partial density of state functions, using either method, show the contribution of the Ca is essentially localised to low frequencies, whilst that from the Ti is essentially flat and extends to a significantly higher frequency. The contribution from the O anions is more structured, showing a sharp rise at ~6 THz, a sharp drop at ~19 THz, followed by a small energy gap and a narrow peak centred on ~23 THz. The expectation values of energy calculated from the partial vibrational density of states are 317 K, 451 K and 620 K for Ca, Ti and O respectively, which agree fairly well with the vibrational Debye temperatures derived from fitting the atomic displacement parameters. The two-term Debye model, either based on the heat capacity or the molar volume fitting, tracks the low frequency part of the *ab-initio* based calculation of the full vibrational density of states out to ~5 THz. The heat capacity based model has a high frequency cut-off at 17.5 THz, just below the lower edge of the energy gap, whilst that derived from the molar volume cuts off at 21.3 THz, just

below the maxima of the small peak that occurs above the gap in the calculated full vibrational density of states.

In the light of these experimental observations based on an $A^{II}B^{IV}O_3$ perovskite in space group *Pbnm*, it would be timely, if experimentally challenging, to carry out a similar investigation of the lower mantle phase $MgSiO_3$ to see whether it behaves in the simple manner suggested by Anderson [26], or whether its behaviour is in fact more subtle, as in the case of $CaTiO_3$.

Acknowledgements

I am grateful to Dr. J.A. Souza (Universidade Federal de Säo Carlos) for providing me the digitised data for the full and partial phonon densities of states functions for $CaTiO_3$. The manuscript was improved by suggestions from two anonymous referees, and Prof. K.H.J. Buschow is thanked for editorial handling of the manuscript.

References

[1] G. Rose, Pogendorff Annalen Physik Chemie 48 (1839) 551.
[2] B.J. Kennedy, C.J. Howard, B.C. Chakoumakos, J. Phys. Condens. Matter 11 (1999) 1479.
[3] R. Ali, M. Yashima, J. Solid State Chem. 178 (2005) 2867.
[4] M. Yashima, R. Ali, Solid State Ionics 180 (2009) 120.
[5] R. Ranjan, D. Pandey, N.P. Lalla, Phys. Rev. Lett. 84 (2000) 3726.
[6] M.A. Carpenter, C.J. Howard, K.S. Knight, Z. Zhang, J. Phys. Condens. Matter 18 (2006) 10725.
[7] I.G. Wood, G.D. Price, J.N. Street, K.S. Knight, Experimental Report RB7844, ISIS 98, The Rutherford Appleton Laboratory ISIS Facility Annual Report 1997–1998, RAL-TR-1998-050.
[8] A.I. Becerro, S.A.T. Redfern, M.A. Carpenter, K.S. Knight, F. Seifert, J. Solid State Chem. 167 (2001) 459.
[9] J.N. Walsh, P.A. Taylor, A. Buckley, T.W. Darling, J. Schreuer, M.A. Carpenter, Phys. Earth Planet. In. 167 (2008) 110–117.
[10] V.V. Lemanov, A.V. Sotnikov, E.P. Smirnova, M. Weihnacht, R. Kunze, Solid State Commun. 110 (1999) 611.
[11] C.J. Ball, R.G. Blake, D.J. Cassidy, J.L. Woolfrey, J. Nucl. Mater. 151 (1988) 151.
[12] T. Sato, Y. Hanajiri, T. Yamashita, T. Matsui, T. Nagasaki, J. Nucl. Mater. 294 (2001) 130.
[13] S. Yamanaka, K. Kurosaki, T. Maekawa, T. Matsuda, S. Kobayashi, M. Uno, J. Nucl. Mater. 344 (2005) 61.
[14] T. Sato, T. Yamashita, T. Matsui, J. Nucl. Mater. 344 (2005) 67.
[15] H. Yang, Y. Ohishi, K. Kurosaki, H. Muta, S. Yamanaka, J. Alloys Compd. 504 (2010) 201.
[16] R.B. Von Dreele, A.C. Larson, Los Alamos National Laboratory Report LAUR 86-748, 1986.
[17] K.S. Knight, Can. Mineral. 47 (2009) 381.
[18] C.J. Ball, G.J. Thorogood, E.R. Vance, J. Nucl. Mater. 190 (1992) 298.
[19] S.A.T. Redfern, J. Phys. Condens. Matter 8 (1996) 8267.
[20] M.A. Carpenter, A.I. Becerro, F. Seifert, Am. Mineral. 86 (2001) 348–363.
[21] D.C. Wallace, Thermodynamics of Crystals, Wiley, New York, 1972.
[22] T.H.K. Barron, CINDAS Data Series on Materials Properties I-4, 1998, 1.
[23] N.L. Ross, R.J. Angel, Am. Mineral. 84 (1999) 277.
[24] B.F. Woodfield, J.L. Sapiro, R. Stevens, J. Boerio-Goates, R.L. Putnam, K.B. Helean, A. Navrotsky, J. Chem. Thermodyn. 31 (1999) 1573.
[25] Y.P. Varshni, Phys. Rev. B 2 (1970) 3952–3958.
[26] O.L. Anderson, Am. Mineral. 83 (1998) 23.
[27] C.J. Howard, H.T. Stokes, Acta Cryst. B54 (1998) 782.
[28] W. Cochran, A. Zia, Phys. Stat. Sol 25 (1968) 273.
[29] C.N.W. Darlington, Acta Cryst. A58 (2002) 299.
[30] K.S. Knight, Can. Mineral., in press.
[31] I.G. Wood, K.S. Knight, G.D. Price, J.A. Stuart, J. Appl. Crystallogr. 35 (2002) 291.
[32] K. Parlinski, Y. Kawazoe, Y. Waseda, J. Chem. Phys. 114 (2001) 2395.
[33] J.A. Souza, J.P. Rino, Acta Mater. 59 (2011) 1409.